INVESTIGATION OF A GAS–PARTICLE FLOW WITH PARTICLE–PARTICLE AND PARTICLE–WALL COLLISIONS BY IMMERSED BOUNDARY METHOD

YUSUKE MIZUNO, TAKUYA INOUE, SHUN TAKAHASHI & KOTA FUKUDA
Tokai University, Japan.

ABSTRACT

We investigated gas–particle flows by using the three-dimensional incompressible Navier–Stokes equation with the immersed boundary method (IBM) to treat particles–wall collisions. We compared flow structures from the two-way coupled simulation with the one-way simulation that is usually used in the industrial simulation. In this study, all objectives, which are particles and walls, are defined by the level-set function for the ghost-cell method of the IBM. The proposed algorithms to represent particle–particle and particle–wall collisions are simple and stable for the coupling simulation. Moreover, flow structures obtained with the coupled simulation of the moving, colliding and rebounding particles are in good agreement with the previous numerical and experimental results. The one-way and two-way coupling simulations were carried out based on a number of particles of 50, 100 and 200, respectively. As a result, the one-way scheme indicated more frequently collisions on the particle and wall than the two-way scheme. The reason is that the one-way scheme ignored the particle–flow interactions.
Keywords: immersed boundary method, particle–wall collisions.

1 INTRODUCTION

Shot peening process is often used for metal surface process for generating a compressible residual stress on the surface, which impacts the surface with a large number of particles shot by a compressible flow [1]. Nguyen *et al*. [1] investigated the location of particle–surface impacts in the multiphase flow simulation. They used the Euler–Lagrange approach and Reynolds-averaged Navier–Stokes equations, which cannot sufficiently model the particle–flow interactions and the detailed flow structures.

We developed the three-dimensional Euler–Euler incompressible flow solver with an immersed boundary method (IBM) for examining the structures and behaviors of particles in the multiple particle–wall collisions. Therefore, the simulation captures the particle–flow interactions and the detailed flow structures by not using the turbulence model.

The aim of this study is to investigate the flows around multiple particle–wall collisions. We compare the two-way coupled simulation with the one-way simulation that is usually used for clarifying the effect of collisions on particle kinematics in industry and investigate the flow around particle–wall collisions.

2 NUMERICAL METHOD

2.1 Governing equations

The governing equations of the present flow solver are the three-dimensional incompressible Navier–Stokes equations and the equation of continuity. No averaging or filtering process is involved and the flows are solved without any turbulence models:

$$\frac{\partial u}{\partial t} + u\frac{\partial u}{\partial x} + v\frac{\partial u}{\partial y} + w\frac{\partial u}{\partial z} = -\frac{1}{\rho}\frac{\partial p}{\partial x} + v\left(\frac{\partial^2 u}{\partial x^2} + \frac{\partial^2 u}{\partial y^2} + \frac{\partial^2 u}{\partial z^2}\right),$$

$$\frac{\partial v}{\partial t} + u\frac{\partial v}{\partial x} + v\frac{\partial v}{\partial y} + w\frac{\partial v}{\partial z} = -\frac{1}{\rho}\frac{\partial p}{\partial y} + v\left(\frac{\partial^2 v}{\partial x^2} + \frac{\partial^2 v}{\partial y^2} + \frac{\partial^2 v}{\partial z^2}\right), \qquad (1)$$

$$\frac{\partial w}{\partial t} + u\frac{\partial w}{\partial x} + v\frac{\partial w}{\partial y} + w\frac{\partial w}{\partial z} = -\frac{1}{\rho}\frac{\partial p}{\partial z} + v\left(\frac{\partial^2 w}{\partial x^2} + \frac{\partial^2 w}{\partial y^2} + \frac{\partial^2 w}{\partial z^2}\right),$$

$$\frac{\partial u}{\partial x} + \frac{\partial v}{\partial y} + \frac{\partial w}{\partial z} = 0, \qquad (2)$$

where u, v, w, p, ρ and v are the fluid velocity, pressure, density, kinematic viscosity, respectively. The fractional step method is applied for time marching. The grid is defined by an equally spaced Cartesian mesh. The convection term is evaluated by the second-order skew–symmetric scheme [2]. The pressure and diffusion term are calculated by the second-order finite-difference method. The Poisson equation of the pressure is calculated by the successive over-relaxation (SOR) method.

2.2 Immersed boundary method

Our flow solver represents objects by the level set and ghost-cell (GC) methods [3]. Each cell is classified as a fluid cell (FC), a GC, or an object cell (OC) by the classification manner of the level set function φ expressed as eqx. (3).

$$0 < \phi_{FC},$$
$$-2\sqrt{3}\Delta x \le \phi_{GC} \le 0, \qquad (3)$$
$$\phi_{OC} < -2\sqrt{3}\Delta x.$$

The GCs are assigned in two layers as shown in Fig. 1. The flow equations in a GC are determined by the flow in an image point within the region occupied by fluid cells. To avoid recursive references, the probe length is set to 1.75 times the mesh size Δx. The primitive
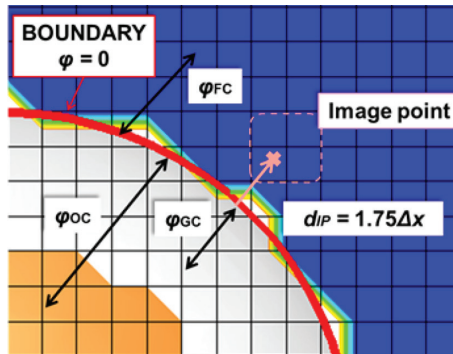

Figure 1: Domain around an object.

variables on the image point are interpolated of the values in the surrounding fluid. Finally, the value of a GC is defined by the value at the image point. To determine the velocity components of the GCs, non-slip boundary conditions are assumed at the object surface. The density and pressure are subjected to Neumann boundary conditions as follows

$$u_{GC} = u_{IP} - \frac{d_{IP} + |\phi_{GC}|}{d_{IP}} \left(u_{IP} - u_{IB} \right),$$

$$v_{GC} = v_{IP} - \frac{d_{IP} + |\phi_{GC}|}{d_{IP}} \left(v_{IP} - v_{IB} \right),$$

$$(4)$$

$$w_{GC} = w_{IP} - \frac{d_{IP} + |\phi_{GC}|}{d_{IP}} \left(w_{IP} - w_{IB} \right),$$

$$P_{GC} = P_{IP}.$$

2.3 The motion of the particle

The particles movements obey Newton's equations for linear and transportation of a rigid body. Note that this simulation ignores the rotation of the particle. The velocities of two particles (labels 1 and 2) after their collision are, respectively, given by

$$\mathbf{u'}_{p,1} = \frac{m_{p,2}}{m_{p,1} + m_{p,2}} (1 + e) \left[\left(\mathbf{u}_{p,2} - \mathbf{u}_{p,1} \right) \cdot \mathbf{c} \right] \mathbf{c} + \mathbf{u}_{p,1},$$

$$(5)$$

$$\mathbf{u'}_{p,2} = \frac{m_{p,1}}{m_{p,1} + m_{p,2}} (1 + e) \left[\left(\mathbf{u}_{p,1} - \mathbf{u}_{p,2} \right) \cdot \mathbf{c} \right] \mathbf{c} + \mathbf{u}_{p,2},$$

where m_p, $\mathbf{u}_p = (u_p, v_p, w_p)$ and e are the mass, velocity of the particle coefficient restitution respectively, and $\mathbf{c}$ is a standardization vector [4, 5]. The collision detection of particles 1 and 2 is determined by Pythagoras' theorem as follows:

$$\sqrt{\left(x_2 - x_1 \right)^2 + \left(y_2 - y_1 \right)^2 + \left(z_2 - z_1 \right)^2} \leq \sqrt{\left(r_1 + r_2 \right)^2}, \tag{6}$$

where r is the particle radius.

After the particle–wall collisions, the particle velocity becomes

$$\mathbf{u'}_p = (1 + e) \left[\left(-\mathbf{u}_p \right) \cdot \mathbf{c} \right] \mathbf{c} + \mathbf{u}_p. \tag{7}$$

To detect collision between a particle and the wall, the central position of the particle and the normal vector are obtained from the level set function. When the image point is appeared in the GC of the other object, the velocity and pressure components are defined by those of the nearest object.

3 RESULTS

3.1 Collision of a moving particle with a wall

To validate the present flow solver, the obtained flow structure around the particle–wall collision is compared with the experimental and numerical results of Eames *et al.* [6] and Vanella *et al.* [7].

In this study, the flow quantities are normalized by the initial velocity of the particle and the particle diameter denoted as D. The computational mesh sizes are fixed at $0.05D$ (fine mesh) and $0.1D$ (coarse mesh), respectively. The computational domain is set to $10D \times 10D \times 10D$.

Figure 2 shows the instantaneous vorticity distributions around the particle colliding with the wall. Panels (a) and (b) show the present results on the coarse and fine meshes, respectively. The distributions in the wake of the particle and between the particle and the wall are in good agreement with previous results [6, 7]. The visualization like the adhesion between the particle and the wall has no effect on the flow phenomena. It is just because of the visualization for the object surface by using the isosurface of the level set function. Figure 3 shows the instantaneous vorticity distributions of the rebounding particle. Panels (a) and (b) show the present results on the coarse
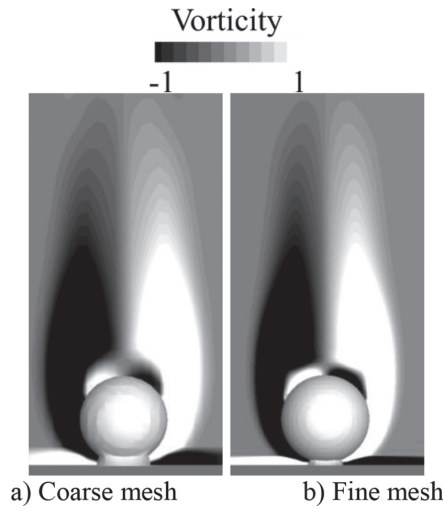

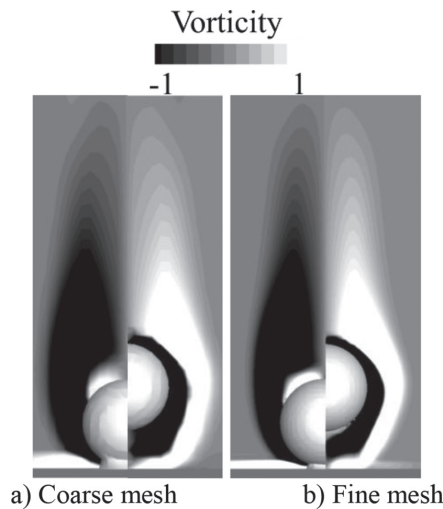Figure 2: Vorticity distribution at the particle–wall collision

Figure 3: Vorticity distributions, at the collision of the particle with the wall (left images) and at the rebound of the particle (right images).

and fine meshes, respectively. The wake vortex is broken by the rebound after the collision. The present distribution in the wake of the rebounding particles is in good agreement with previous result [7].

3.2 Collision of a multiple particles with a wall

The present flow solver is applied to the flow around multiple particles colliding with a wall. The Reynolds number is set to 400, based on the particle diameter and the relative velocity between the freestream and the particle during its impact with the wall. The grid size is fixed
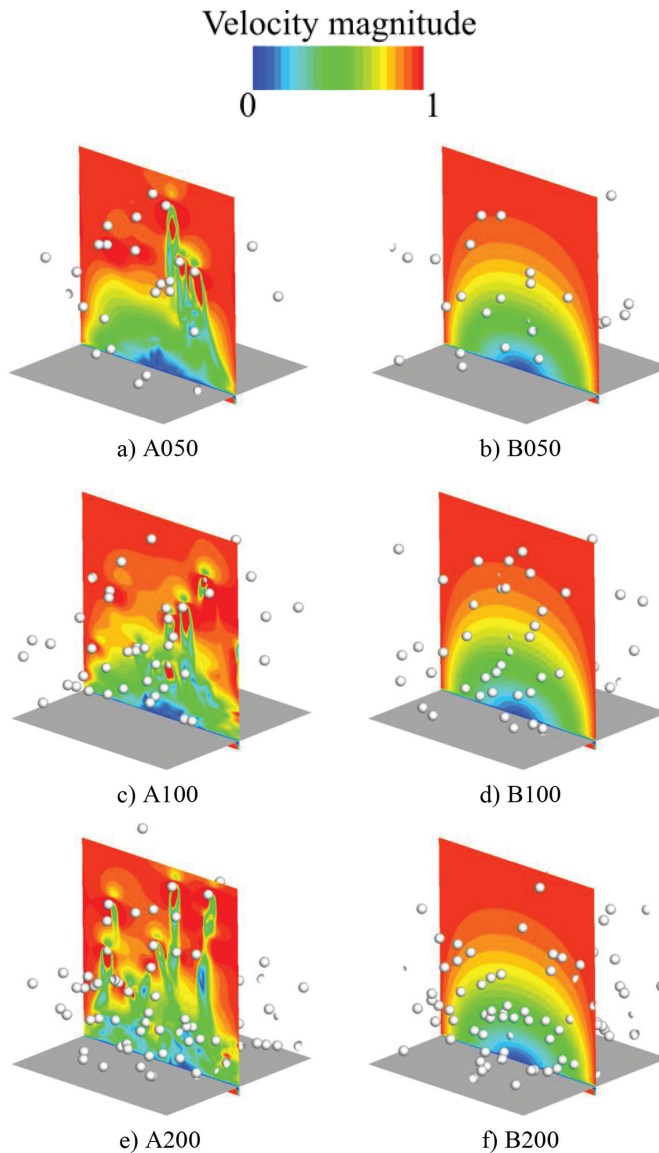

Figure 4: Flow distributions at $t^* = 40$. The color map shows the velocity magnitude.
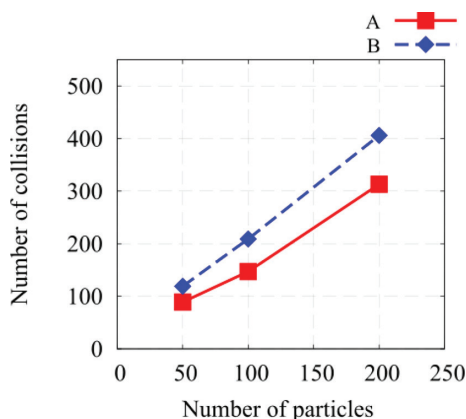
Figure 5: Number of collisions of the wall and the multiple particles. Red and blue plots are obtained in scheme (A) and (B), respectively.

at 0.1D. The computational domain is sized as $20D \times 20D \times 21D$, and the wall is fixed at $z = 1D$ location. The number of particles is set to 50, 100 or 200. All particles are assumed as same sized, hard steel particles with deformation. The initial position of the multiple particles is randomly located in the out of the computational domain. The two schemes are compared in this simulation; the two-way (A) and one-way (B) schemes. In the scheme (B), the initial flow condition is steady flow.

Figure 4 shows the instantaneous distributions of the velocity magnitudes at the center of the computational domain at nondimensional time $t^* = 40$. In scheme (A), the flow structure becomes more complicated by the influences of the particles in the fluid. Furthermore, when the number of particles becomes large, the complexity is enhanced. On the other hand, in scheme (B), the flow distributions are steady because this scheme excludes the influence of the particles on the flow. Although the initial particle positions are same both scheme (A) and (B), the particle distributions are clearly different due to the effect of the interaction between the particle and the flows.

Figure 5 plots the number of particle–wall collisions as functions of particle number in scheme (A) and (B). The scheme (B) estimates larger number of collisions than the scheme (A). Moreover, the overestimation is enhanced with the increase of the particle number. In scheme (B), the particles move laterally because of the steady flows even in the vicinity of the wall. The steady flow without any wake vortex and the pressure recovery make the particles collide to the wall and each other.

4 CONCLUSIONS

Flows around multiple particles colliding with a wall are investigated by a three-dimensional flow solver based on IBM. The wake structures of the particle colliding with the wall showed the same tendency with previous studies. The differences between the two-way and one-way schemes were explored for multiple particles colliding with the wall. When the number of the particles becomes large, more complicated flow structure was observed in the two-way scheme since the one-way scheme could not accurately predict the flow. Consequently, the one-way scheme overestimated the number of collisions due to the steady flow without the influence of the particles on the fluid.

REFERENCES

[1]   Nguyen, V.B., Poh, H.J. & Zhang, Y.W., Predicting shot peening coverage using multi-phase computational fluid dynamics simulations. *Powder Technology*, **256**, pp. 100–112, 2014.
https://doi.org/10.1016/j.powtec.2014.01.097

[2]   Morinishi, Y., Skew–symmetric form of convective terms and fully conservative finite difference schemes for variable density low–Mach number flows. *Journal of Computational Physics*, **229**, pp. 276–300, 2010.
https://doi.org/10.1016/j.jcp.2009.09.021

[3]   Mizuno, Y., Takahashi, S., Nonomura, T., Nagata, T. & Fukuda, K., A simple immersed boundary method for compressible flow simulation around a stationary and moving sphere. *Mathematical Problems in Engineering*, **2015**, pp. 1–17, 2015.
https://doi.org/10.1155/2015/438086

[4]   Kosinski, P. & Hoffmann, C.A., Extension of the hard-sphere particle-wall collision model to account for particle deposition. *Physical Review E*, **79**, pp. 1–11, 2009.
https://doi.org/10.1103/physreve.79.061302

[5]   Kosinski, P. & Hoffmann, C.A., An extension of the hard–sphere particle–particle collision model to study agglomeration. *Chemical Engineering Science*, **65**, pp. 3231–3239, 2010.
https://doi.org/10.1016/j.ces.2010.02.012

[6]   Eames, I. & Dalziel, S.B., Dust resuspension by the flow around an impacting sphere. *Journal Fluid Mechanics*, **403**, pp. 305–328, 2000.
https://doi.org/10.1017/s0022112099007120

[7]   Vanella, M. & Balaras, E., A moving-least-squares reconstruction for embedded–boundary formulations. *Journal of Computational Physics*, **228**, pp. 6617–6628, 2009.
https://doi.org/10.1016/j.jcp.2009.06.003